Phase transitions in Ehrenfest urn model with interactions: Coexistence of uniform and nonuniform states

Chi-Ho Cheng,[1,*] Beverly Gemao [2,3] and Pik-Yin Lai [2,†]

[1]*Department of Physics, National Changhua University of Education, Changhua 500, Taiwan, Republic of China*
[2]*Department of Physics and Center for Complex Systems, National Central University, Chung-Li District, Taoyuan City 320, Taiwan, Republic of China*
[3]*Physics Department, MSU-Iligan Institute of Technology, 9200 Iligan City, Philippines*

A model based on the classic noninteracting Ehrenfest urn model with two urns is generalized to M urns with the introduction of interactions for particles within the same urn. As the inter-particle interaction strength is varied, phases of different levels of nonuniformity emerge and their stabilities are calculated analytically. In particular, coexistence of locally stable uniform and nonuniform phases connected by first-order transition occurs. The phase transition threshold and energy barrier can be derived exactly together with the phase diagram obtained analytically. These analytic results are further confirmed by Monte Carlo simulations.

I. INTRODUCTION

In 1872, when Boltzmann formulated the H-theorem [1] to explain how a system approaches equilibrium from nonequilibrium and the irreversibility associated with the second law of thermodynamics, it also led to the microscopic time reversal and the Poincaré recurrence paradoxes [2], which were not fully understood at that time. Decades later, the Ehrenfest two-urn model [3] was proposed in 1907 to resolve the paradoxes and clarify the relationship between reversible microscopic dynamics and irreversible thermodynamics. The classic Ehrenfest model [3] considered a total of N particles distributed in two urns with each particle in an urn to be chosen randomly and put into the other with equal probability. The Ehrenfest urn model is a simple and tractable model to understand or illustrate the conceptual foundation of statistical mechanics and the relaxation to equilibrium. This model was solved exactly by Kac [4] and has been often used to demonstrate the second law of thermodynamics and the approach to equilibrium.

Later on, the Ehrenfest model was generalized to the case of unbalanced jumping rates between the two urns [5,6]. The two-urn Ehrenfest model was subsequently extended to multiurn systems [7–10] to investigate the associated nonequilibrium steady states. Its various generalizations have been applied to investigate a variety of nonequilibrium phenomena. The continuous time limit of the evolution of the population probability state led to a linear Fokker- Planck equation [4,11] which was further modified to incorporate the nonlinear contribution [12–14], which is motivated by the processes associated with anomalous-diffusion phenomena [15–17]. The associated generalized H theorem for the nonlinear

Fokker-Planck equation was also studied [18–22]. However, most of such generalization is non-interacting, or the inclusion of interaction is phenomenological and not explicit. Until recently, the two-urn Ehrenfest model was extended to include particle interactions inside an urn [23]. In the two-urn Ehrenfest model with interaction, particles can interact with all other particles inside the same urns, but particles belonging to different urns do not interact. In addition, a jumping rate (asymmetric in general) from one urn to another is introduced, which is independent of the particle interaction. The system can exhibit interesting phase transitions and the Poincaré cycle and relaxation times can be calculated [23].

In this paper, we extend the interacting Ehrenfest model to M urns ($M > 2$). In particular, we focus on the equilibrium case when detailed balance can be achieved. A possible application for the present equilibrium model and its generalization is the optimization in partitioning problem [24,25], such as distributing a fixed amount of total resource to M locations with a certain cost to be minimized. The equilibrium phase behavior of the model is rather rich and can be investigated in detail. Analytic and exact results are derived for the conditions of the emergence of coexistence of uniform or nonuniform phases and the associated first-order phase transition and energy barrier. Monte Carlo simulations are also performed to verify our theoretical findings.

II. THE *M*-URNS MODEL WITH INTERACTIONS

The two-urn interacting model in Ref. [23] is extended to the case of M urns. Similar to the two-urn case [23], N particles are distributed into the M urns ($M \geqslant 3$ is considered in this paper). Pairwise all-to-all interaction is introduced only for particles in the same urn and particles in different urns do not interact. Besides particle interactions, direct jumping rates are further introduced between a pair of urns. In general, these jump rates can be asymmetric (unbalanced) and the system is

———————
*phcch@cc.ncue.edu.tw
†pylai@phy.ncu.edu.tw

012123-1

nonequilibrium with nonzero net particle fluxes. On the other hand, if the particles in any urn are free to make transitions back and forth with another urn with balanced jump rates such that detailed balance is obeyed, the system can achieve an equilibrium state. In this paper, we will focus on such an equilibrium situation and the associated phase transition.

The energy or Hamiltonian of the interacting particles in the urns are given by

$$\beta \mathcal{H} = \frac{1}{2N} \sum_{i=1}^{M} g_i n_i (n_i - 1), \tag{1}$$

where $\beta \equiv 1/(k_B T)$ is the inverse temperature and g_i is the pairwise interaction (in unit of $k_B T$) of the particles inside the ith urn. The urns can be thought of as arranged in some periodic lattice, such as a one-dimensional ring, a completely connected network, or in any undirected network such that the jump rates between neighboring urns are balanced. Under such conditions, with a suitable choice of transition dynamics, such as the Metropolis rule, detailed balance is obeyed and the system can achieve thermal equilibrium with the equilibrium population distribution in the urns being Boltzmann, given by

$$\rho_{\text{eq}}(\vec{n}) \propto \frac{N!}{\prod_{i=1}^{M} n_i!} e^{-\beta \mathcal{H}} \propto \frac{N!}{\prod_{i=1}^{M} n_i!} e^{-\frac{1}{2N} \sum_{i=1}^{M} g_i n_i (n_i - 1)}, \tag{2}$$

where $\vec{n} \equiv (n_1, \cdots, n_M)^{\mathsf{T}}$. The fraction of particles in the ith urn is denoted by x_i, with the constraint $\sum_{i=1}^{M} x_i = 1$. In the large $N \to \infty$ limit, using Stirling approximation and with the fraction $x_i \equiv \frac{n_i}{N}, \vec{x} \equiv (x_1, \cdots, x_{M-1})^{\mathsf{T}}$, and $x_M = 1 - x_1 - x_2 - \cdots - x_{M-1}$, one has

$$\rho_{\text{eq}}(\vec{x}) = \mathcal{N} \frac{e^{N f(\vec{x})}}{\sqrt{\prod_{i=1}^{M} x_i}}, \tag{3}$$

where

$$f(\vec{x}) = -\sum_{i=1}^{M-1} \left(x_i \ln x_i + \frac{g_i}{2} x_i^2 \right) - \left(1 - \sum_{i=1}^{M-1} x_i \right)$$

$$\times \ln \left(1 - \sum_{i=1}^{M-1} x_i \right) - \frac{g_M}{2} \left(1 - \sum_{i=1}^{M-1} x_i \right)^2 \tag{4}$$

and

$$\mathcal{N}^{-1} \equiv \int_{\sum_{i=1}^{M-1} x_i \leqslant 1} \prod_{i=1}^{M-1} dx_i \frac{e^{N f(\vec{x})}}{\sqrt{\prod_{i=1}^{M} x_i}}. \tag{5}$$

The saddle point, $\vec{x}^*$, is obtained from $\partial f/\partial x_\alpha|_{\vec{x}^*} = 0, \alpha = 1, 2, \cdots, M - 1$, which leads to the saddle-point equations

$$x_i^* e^{g_i x_i^*} = \text{the same constant}, \quad i = 1, 2, \cdots, M \tag{6}$$

$$\sum_{i=1}^{M} x_i^* = 1, \quad 0 < x_i^* < 1. \tag{7}$$

Hereafter, unless otherwise stated, we shall consider the case of identical pairwise interactions for all the urns, i.e., $g_i = g$ for $i = 1, 2, \cdots, M$.

A. Uniform and nonuniform equilibrium states

Since $g_i = g$ for every urn, the uniform solution of $\vec{x}^{(0)} \equiv (\frac{1}{M}, \cdots, \frac{1}{M})^{\mathsf{T}}$ is always a saddle-point solution of Eqs. (6). In addition, M nonuniform saddle points (related by symmetry) with different values for x_i^* can exist. Notice that the saddle points are also the fixed points in the corresponding dynamical system which describes the general nonequilibrium physics of the system. Since the function xe^{gx} is monotonic increasing in the domain $0 \leqslant x \leqslant 1$ for $g \geqslant -1$, all x_i^* satisfying Eqs. (6) can take one possible value and hence only the uniform state is possible. On the other hand, the function has one peak in $0 \leqslant x \leqslant 1$ for $g < -1$, thus each x_i^* [satisfying Eqs. (6) with $g_i = g$] can take one of the two possible values, allowing the possibility of a nonuniform solution in Eqs. (6). Therefore, if n urns have the fraction being one of the roots, say x, the other $M - n$ urns will take the fraction $(1 - nx)/(M - n)$. Hence one can derive an equation for the saddle point(s),

$$xe^{gx} = \frac{(1 - nx)}{M - n} e^{\frac{g(1 - nx)}{M - n}}, \quad n = 0, 1, \cdots, M - 1, \tag{8}$$

which can also be written as

$$\frac{1}{x} = n + (M - n) e^{g \frac{Mx - 1}{M - n}}. \tag{9}$$

$n = 0$ represents uniform distribution $(\vec{x}^{(0)})$ of particles in which all M urns have the same fraction of $1/M$. n corresponds to the number of urns having the same fraction (say x) and the other $M - n$ urns having the same fraction of a different value $(\frac{1 - nx}{M - n})$. Notice that $x = 1/M$ is always a solution in Eqs. (8). It is also easy to see that if x is the root of Eqs. (8) for $n = k \geqslant 1$, then $\frac{1 - kx}{M - k}$ is also a root for $n = M - k$. Hence n and $M - n$ have the same saddle points and it is sufficient to consider $k = 0, 1, \cdots, \lfloor \frac{M}{2} \rfloor$ different states, where $k = 0$ is the uniform state and the others $k = 1, \cdots, \lfloor \frac{M}{2} \rfloor$ are nonuniform states with different levels of nonuniformity.

B. Saddle-node bifurcations for the nonuniform saddle points

Now consider first the simpler case of $M = 3$; take, for example $n = 2$ in Eqs. (8) with the saddle point $(x_1, x_2) = (x, x)$, where x is given by the roots of

$$xe^{gx} = (1 - 2x)e^{g(1 - 2x)}. \tag{10}$$

The stability of the saddle point is determined by the 2×2 Hessian matrix of f in Eq. (4):

$$\mathbf{f}'' = - \begin{pmatrix} 2g + \frac{1}{x} + \frac{1}{1 - 2x} & g + \frac{1}{1 - 2x} \\ g + \frac{1}{1 - 2x} & 2g + \frac{1}{x} + \frac{1}{1 - 2x} \end{pmatrix}. \tag{11}$$

The saddle point is stable if $\text{Tr} \mathbf{f}'' < 0$ and $\det \mathbf{f}'' > 0$, i.e., the real part of the two eigenvalues of $\mathbf{f}''$ are both negative. Using Eq. (11), one can show that the uniform $(x_1, x_2) = (1/3, 1/3)$ saddle point is stable for $g > -3$. On the other hand, careful examination reveals that $x = \frac{1}{3}$ is always a root in Eq. (10) and two smaller roots emerge in a pair (one stable and one unstable) for some negative values of $g < g_c$, characteristics of a saddle-node bifurcation. At the bifurcation point, g_c can be determined by the condition of emergence of the pair of

(stable and unstable) fixed point together with the condition

$$(xe^{gx})' = [(1 - 2x)e^{g(1-2x)}]'. \qquad (12)$$

x can be eliminated from Eqs. (10) and (12), then g_c is simply given by the root of the following transcendental equation:

$$1 - \sqrt{1 + \frac{8}{3g}} = 2\left(1 + \sqrt{1 + \frac{8}{3g}}\right)$$
$$\times \exp\left[\frac{g}{4}\left(1 + 3\sqrt{1 + \frac{8}{3g}}\right)\right], \qquad (13)$$

which has only a single root of $g_c = -2.74564...$. In fact, for $g < g_c$, three other stable saddle points related by symmetry emerge in the x_1-x_2 phase plane. See Fig. 5 for the Monte Carlo simulation results displaying $\rho_{eq}(x_1, x_2)$ in the coexisting regime. Thus, a stable nonuniform equilibrium state exists for $g < g_c$, a stable uniform equilibrium state exists for $g > -3$, and bistable coexisting equilibrium states of uniform and nonuniform populations occur for $-3 < g < g_c$.

For M urns, the condition of saddle-node bifurcation is obtained by equating the slopes of the left- and right-hand sides of Eqs. (8) and, using Eqs. (8), one can derive

$$1 + gx + nx\left(\frac{g}{M-n} + \frac{1}{1-nx}\right) = 0. \qquad (14)$$

Equations (8) and (14) will determine the critical value $g_c(n)$ for the new fixed points to emerge via saddle-node bifurcations. For $n = 0$, $x = -1/g$ is the solution of Eq. (14) and

$$x = \frac{1}{2n}\left[1 \pm \sqrt{1 + \frac{4n(M-n)}{gM}}\right] \quad \text{for } n = 1, 2, \cdots, M - 1. \qquad (15)$$

The threshold values g_c at which new fixed-point solutions emerge can be obtained by substituting the solution for x in Eq. (15) back to Eqs. (8) to give $g_c(n = 0) = -M$ and for $n > 0$, $g_c(n)$ is given by the root of the following transcendental equation:

$$1 + \text{sgn}\left(\frac{M}{2} - n\right)\sqrt{1 + \frac{4n(M-n)}{gM}} = \frac{n}{M-n}\left(1 - \text{sgn}\left(\frac{M}{2} - n\right)\right)\sqrt{1 + \frac{4n(M-n)}{gM}}$$
$$\times \exp\left[\frac{g}{M-n}\left(1 - \frac{M}{2n}\left(1 + \text{sgn}\left(\frac{M}{2} - n\right)\sqrt{1 + \frac{4n(M-n)}{gM}}\right)\right)\right], \qquad (16)$$

where

$$\text{sgn}(x) \equiv 1 \text{ for } x \geqslant 0, -1 \text{ for } x < 0. \qquad (17)$$

Notice that $n = k$ and $n = M - k$ ($k \geqslant 1$) have the same g_c and hence the (nonuniform) fixed points emerge together via saddle-node bifurcation. Furthermore, for $n = M/2$ (i.e., even M), the only solution to Eqs. (8) and (14) is $g_c = -M$ and $x = 1/M$, and hence there is no nonuniform fixed point emerging due to saddle-node bifurcation. This special nonuniform fixed point emerges at $g_c = -M$ via pitchfork bifurcation for even M, but careful examination of the Hessian matrix Eq. (21) reveals that this saddle point is unstable. Thus, the number of distinct g_c's is $\lfloor \frac{M}{2} \rfloor$, and the number of distinct nonuniform phases (only 1 stable and the rest are unstable, as shown below) is $M - 1$.

C. Stability for the saddle points

The stability condition of the saddle point $\vec{x}^*$ is determined by the $(M - 1) \times (M - 1)$ Hessian matrix $(\mathbf{f}'')_{\alpha\beta} \equiv \frac{\partial^2 f}{\partial x_\alpha \partial x_\beta}|_{\vec{x}^*}$. Direct calculations give

$$\frac{\partial^2 f}{\partial x_\alpha \partial x_\beta}\bigg|_{\vec{x}^*} = -\left(\frac{1}{x_M} + g\right) - \left(\frac{1}{x_\alpha} + g\right)\delta_{\alpha\beta},$$
$$x_M \equiv 1 - x_1 - x_2 - \cdots, x_{M-1}. \qquad (18)$$

For the uniform saddle point $\vec{x}^{(0)} \equiv (\frac{1}{M}, \cdots, \frac{1}{M})^{\intercal}$,

$$\frac{\partial^2 f}{\partial x_\alpha \partial x_\beta}\bigg|_{\vec{x}^{(0)}} = -(M + g)(1 + \delta_{\alpha\beta}), \qquad (19)$$

whose eigenvalues are $-M(g + M)$ and $-(g + M)$ (with $(M - 2)$ degeneracy). Thus the uniform phase becomes unstable for $g < -M$, i.e., when the interparticle attraction is strong enough, the uniform phase becomes unstable.

For the first nonuniform saddle point $\vec{x}^{(1)} \equiv (y, \cdots, y)^{\intercal}$, $y \neq \frac{1}{M}$ and y is the root of Eqs. (8) with $n = M - 1$ or $n = 1$, we have from Eqs. (18)

$$\frac{\partial^2 f}{\partial x_\alpha \partial x_\beta}\bigg|_{\vec{x}^{(1)}} = -\left(\frac{1}{1 - (M-1)y} + g\right) - \left(\frac{1}{y} + g\right)\delta_{\alpha\beta}, \qquad (20)$$

whose eigenvalues are $-(Mg + \frac{1}{y[1-(M-1)y]})$, and $-(g + \frac{1}{y})$ [with $(M - 2)$ degeneracy].

In the case of even M, the nonuniform saddle point $\vec{x}^{(\frac{M}{2})} \equiv (y, \cdots, y, \frac{2}{M} - y, \cdots, \frac{2}{M} - y)$ exists, where y is the root in Eqs. (8) with $n = \frac{M}{2}$, the Hessian matrix is

$$\frac{\partial^2 f}{\partial x_\alpha \partial x_\beta}\bigg|_{\vec{x}^{(\frac{M}{2})}} = \begin{cases} -\left(\frac{M}{2-My} + g\right) - \left(\frac{1}{y} + g\right)\delta_{\alpha\beta} & \text{if } \alpha, \beta \leqslant \frac{M}{2} \\ -\left(\frac{M}{2-My} + g\right)(1 + \delta_{\alpha\beta}) & \text{otherwise.} \end{cases} \qquad (21)$$

The eigenvalues of Eq. (21) are $-(\frac{M}{2-My} + g)$ [with $(\frac{M}{2} - 2)$ degeneracy], $-(g + \frac{1}{y})$ [with $(\frac{M}{2} - 1)$ degeneracy], and $-\frac{1}{2}[M(\frac{M}{2-My} + g) + g + \frac{1}{y} \pm \sqrt{M(M-2)(\frac{M}{2-My} + g)^2 + (\frac{1}{y} + g)^2}]$.
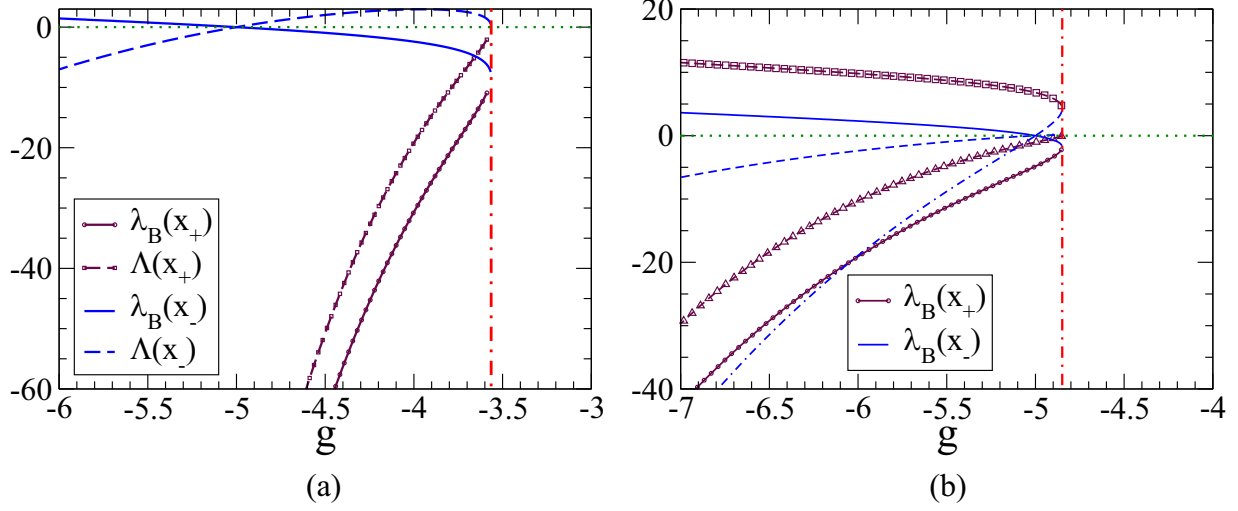
FIG. 1. The eigenvalues as a function of g in a $M = 5$ system for (a) the first nonuniform state (solid curve with degeneracy $M - 2$ and a nondegenerate one denoted by the dashed curve). (b) The second ($k = 2$) nonuniform state (solid curve with degeneracy $M - 3$ and two nondegenerate ones with dashed and dotted curves). The two different colors (brown with symbols and blue without symbol) denote the two nonuniform saddle points x_+ and x_-, respectively. The value of g_c is marked by a vertical dot-dashed line, and the horizontal dotted line marks the zero value.

The kth ($k \geqslant 1$) nonuniform saddle point can be obtained by putting $n = M - k$ in the saddle point Eq. (9). Apart from the uniform saddle point, there are, in general, two nonuniform roots from Eq. (9), except for $k = \frac{M}{2}$ (even M) in which there is only 1 nonuniform root. The eigenvalues of the nonuniform saddlepoints can be evaluated as a function of g to reveal the stability of the nonuniform phases (see Appendix for detail calculations). Careful examination of the eigenvalues indicated that only one of the first nonuniform phases is stable and all other nonuniform ($k > 1$) phases always have at least one eigenvalue with a positive real part. Figure 1 illustrates the results of eigenvalues for the first two nonuniform phases for the case of $M = 5$. Only one of the first nonuniform phases has all its eigenvalues negative for all ranges of g, as depicted in Fig. 1(a) for the case of $M = 5$. For the second nonuniform phase, there is always a positive eigenvalue for both saddle points in the relevant range of g and hence is an unstable nonuniform phase [see Fig. 1(b)]. It should be noted that one can also employ a dynamical model of the form $\frac{d\vec{x}}{dt} = \vec{A}(\vec{x})$, whose fixed points are identical with the saddle point of $f(\vec{x})$. And the stability of the fixed points deduced from the Jacobian matrix $\frac{\partial \vec{A}}{\partial \vec{x}}|_{\vec{x}^*}$ is the same as obtained from the Hessian matrix $\frac{\partial^2 f}{\partial x_\alpha \partial x_\beta}|_{\vec{x}^*}$.

III. FIRST-ORDER PHASE TRANSITION BETWEEN UNIFORM AND FIRST NONUNIFORM STATES

For equilibrium transition between the coexisting uniform and first nonuniform states as g varies, it is convenient to project onto some line in the phase space and consider the projected equilibrium distribution function $\hat{\rho}_{\text{eq}}(x)$ parametrized by a single variable x. For instance, with $M = 3$, one can

define

$$\hat{\rho}_{\text{eq}}(x_1) = \int \rho_{\text{eq}}(x_1, x_2)\delta(x_2 - x_1)dx_2 \propto \frac{e^{Nf(x_1, x_1)}}{\sqrt{x_1(1 - 2x_1)}},$$

(22)

which has two maxima at $1/3$ and $\tilde{x} < 1/3$. A first-order transition occurs at $g = g_t$, which is given by

$$\frac{\partial}{\partial x}\left(\frac{e^{Nf(x, x)}}{\sqrt{x(1 - 2x)}}\right)\Bigg|_{\tilde{x}} = 0$$

(23)

$$\frac{e^{Nf(\frac{1}{3}, \frac{1}{3})}}{\frac{1}{3}\sqrt{\frac{1}{3}}} = \frac{e^{Nf(\tilde{x}, \tilde{x})}}{\sqrt{\tilde{x}(1 - 2\tilde{x})}}.$$

(24)

For $N \to \infty$, one can solve to get $\tilde{x} = \frac{1}{6}$ and

$$g_t = -4\ln 2 = -2.77259...$$

(25)

At $g = g_t$, $\hat{\rho}_{\text{eq}}(x)$ has a local minima at $x = \frac{1}{4}$ which in turn gives the energy barrier at the transition, $\frac{E_b}{N} = \ln 3 - \frac{19}{12}\ln 2 = 0.00112925...$

In general, for M urns, a first-order transition occurs at $g = g_t$, which is given by

$$\frac{e^{Nf(\tilde{\vec{x}})}}{\sqrt{\tilde{x}^{M-1}[1 - (M - 1)\tilde{x}]}} = \frac{e^{Nf(\vec{x}^{(0)})}}{\sqrt{\frac{1}{M^M}}},$$

(26)

$$\frac{\partial}{\partial x}\left(\frac{e^{Nf(\vec{x})}}{\sqrt{x^{M-1}[1 - (M - 1)x]}}\right)\Bigg|_{\tilde{x}} = 0 \qquad \tilde{x} \neq \frac{1}{M}.$$

(27)

For $N \to \infty$, one can solve the above equations to get

$$\tilde{x} = \frac{1}{M(M - 1)},$$

(28)

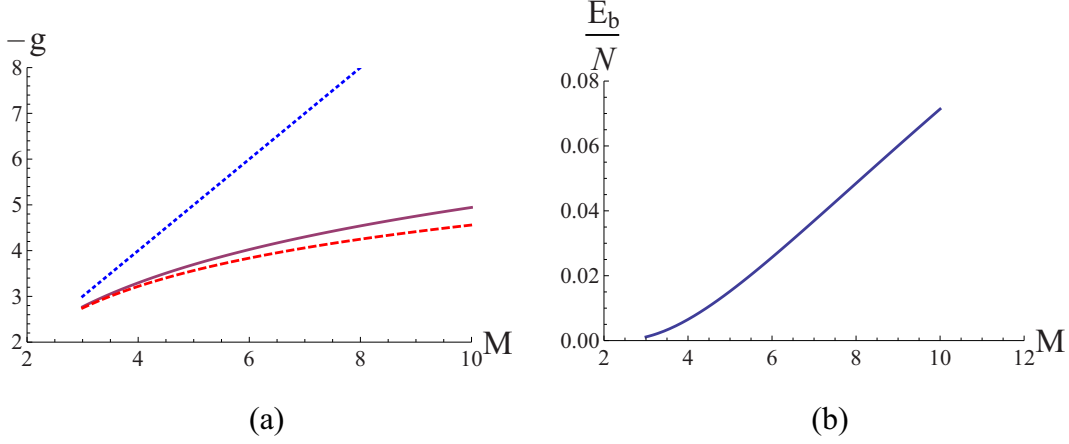$$g_t = -\frac{2(M - 1)}{M - 2}\ln(M - 1).$$

(29)

(a)

(b)

FIG. 2. (a) The threshold g_t for first-order transitions between $0 \leftrightarrow 1$ (solid curve) and the critical value of g at which the locally stable first nonuniform phase emerges, $g_c(n=1)$ (dashed curve), plotted as a function of M. The dotted line denotes $g = -M$ at which the uniform phase becomes unstable. (b) Energy barrier E_b/N vs M for the first-order transitions in (a).

At $g = g_t$, one can define $\hat{\rho}_{eq}(x) \equiv \rho_{eq}(x, \cdots, x)$ to characterize the energy barrier. $\hat{\rho}_{eq}(x)$ has a local minima at $x = \frac{1}{2(M-1)}$, which in turn gives the energy barrier at the transition:

$$\frac{E^b}{N} = \ln \frac{M}{2} - \frac{3M-2}{4M} \ln(M-1). \qquad (30)$$

Figure 2(a) plots the first-order transition threshold as a function of M, together with g_c at which the first nonuniform phase emerges. The characteristic energy barrier at the first-order transition as a function of M is shown in Fig. 2(b).

IV. EQUILIBRIUM PHASE DIAGRAM

As the interparticle attraction becomes stronger (g becomes more negative), the system undergoes a first-order transition from the uniform phase with the emergence of coexisting a locally stable nonuniform phase at $g = g_c(n=1)$. As g becomes more negative, various other nonuniform phases emerge, albeit not locally stable. As g decreases to $g = -M$, the uniform phase becomes unstable and only the stable first nonuniform phase remains. Figure 3 displays the phase diagrams for odd ($M = 7$) and even ($M = 8$) values of M. The values of g_c's at which various nonuniform phases emerge are calculated analytically. The first-order transition point g_t as given by Eq. (29) is also shown.

V. MONTE CARLO SIMULATIONS

To explicitly verify the theoretical results in previous sections, we carry out Monte Carlo simulations for the M urns system. In the simulation, a total of N (N is an integer multiple of M) particles are in the system consisting of M urns and the population of the i urn is denoted by n_i. The transition probability that a particle from the ith urn jumps to the jth urn is

$$T_{i \to j} = \frac{1}{1 + e^{-\frac{g}{N}(n_i - n_j - 1)}}. \qquad (31)$$

It is easy to see that detailed balance is obeyed with the above transition probability and equilibrium will be achieved after sufficient Monte Carlo steps.

In principle, since we are interested in the equilibrium properties, the urns can be placed on any bidirectional network with balanced jump rates between all connected pairs of
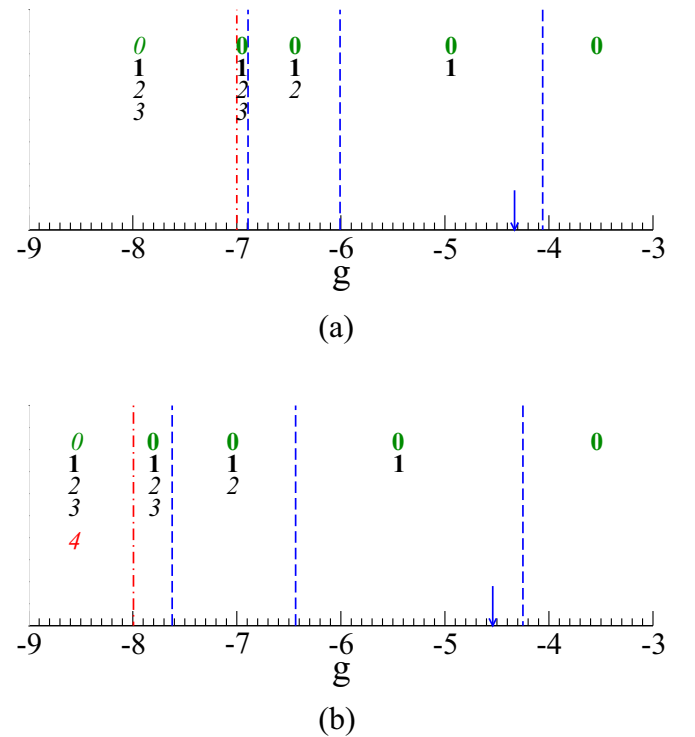

(a)

(b)

FIG. 3. Phase diagrams for (a) $M = 7$ and (b) $M = 8$ showing various phases. Uniform state is denoted by 0 and various nonuniform states of different degree of nonuniformity are denoted by 1, 2,..., with decreasing nonuniformity. A state with a locally stable phase is labeled with a bold font. The most nonuniform ($k = 1$) state always has a stable phase. The thermal first-order phase transition that occurs at g_t is marked by an arrow.
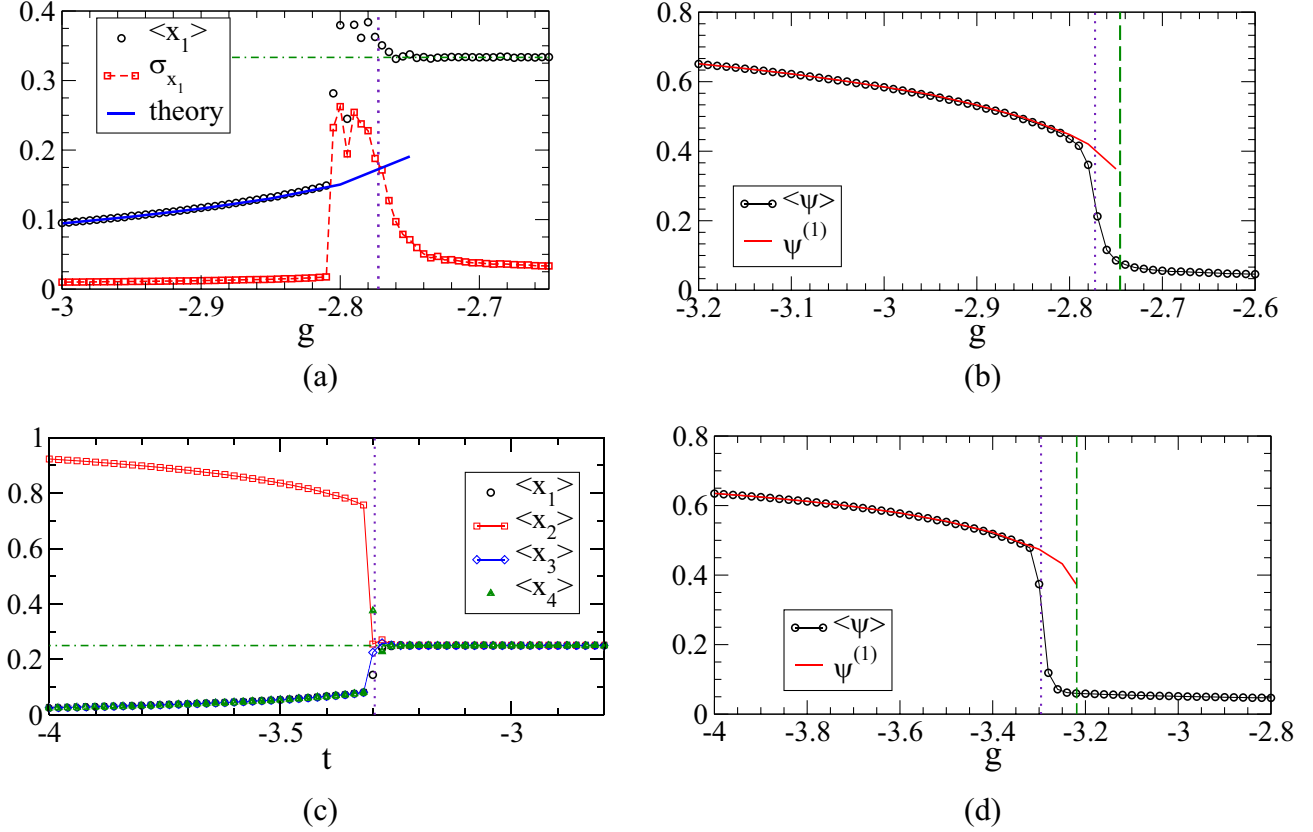
FIG. 4. Monte Carlo simulation results of the urn model for at equilibrium. (a) Three-urn system with $N = 3000$. The mean population and its fluctuation of one of the urns vs g. The urn with lowest population in the nonuniform state is chosen. Solid curve is the theoretical value of the mean population which is obtained from the smallest root of the saddle-point Eq. (9). The theoretical first-order transition point is marked by a vertical dotted line. The uniform state with population fraction of $\frac{1}{3}$ is marked by a horizontal dot-dashed line. 10^5 MCS/N are used in the sampling. (b) The mean nonuniformity as a function of g in (a). The theoretical nonuniformity of the first nonuniform state given by Eq. (A5) is also shown (solid curve). The vertical dashed line marks the theoretical value at which the nonuniform (metastable) state emerges. (c) Four-urn system with $N = 1000$. The mean populations of the urns vs g. The theoretical first-order transition point is marked by a vertical dotted line. The uniform state with population fraction of $\frac{1}{4}$ is marked by a horizontal dot-dashed line. 2×10^5 MCS/N are used in the sampling. (d) The mean nonuniformity as a function of g in (c). The theoretical nonuniformity of the first nonuniform state given by Eq. (A5) is also shown (solid curve). The vertical dashed line marks the theoretical value at which the nonuniform (metastable) state emerges.

urns and particle transition rules made to satisfy the detailed balance condition such that there is vanishing net particle flux between every connected pair of urns.

A particle is chosen at random out of all the particles in the M urns (say the ith urn is chosen) and a transition jump is made according to the probability given in Eq. (31). In practice, for the purpose of investigating equilibrium properties, we put the M urns on a one-dimensional ring for simplicity. For urns on a one-dimensional ring, the possible transitions are $j = i \pm 1$ with equal jump rate to the left and right urns. After some long transient time for equilibration, the populations in each urn or the fraction $x_i(t)$ is recorded for a long sampling time. Time is in Monte Carlo steps per particle (MCS/N). One MCS/N means that on average every particle has attempted a jump.

To quantify how nonuniform the state is, we define

$$\psi = \sqrt{\frac{1}{M(M-1)} \sum_{i \neq j} (x_i - x_j)^2} \qquad (32)$$

as the nonuniformity of the state. ψ can also serve as an order parameter for the phase transition: $\psi \simeq 0$ for the uniform (disordered) state and $\psi > 0$ for the nonuniform (order) state. ψ can be calculated for states of different degrees of nonuniformity (labeled by k) as given by Eq. (A5). One can see that from Eq. (A5) that ψ decreases monotonically with k and thus $k = 1$ is the most nonuniform phase.

Monte Carlo simulations for the three-urn and four-urn systems as a function of g were carried out results are shown in Fig. 4. Figure 4(a) shows the mean population fraction (x_1) of one of the three urns drops from the uniform value of $\frac{1}{3}$ to a smaller value as the interparticle attraction increases. The fluctuation of the population fraction, measured by the variance of x_1, also shows a peak across the expected first-order transition point. The mean nonuniformity of the system $\langle \psi \rangle$ also increases as g decreases across the transition. The analytical nonuniformity of the first nonuniform state $\psi^{(1)}$ is also shown [see Fig. 4(b)]. For interparticle attraction stronger than $|g_c|$ (marked by vertical dashed line), the first nonuniform phase emerges, coexisting with the uniform state. Figure 4(c) shows the mean population fractions of all the urns as a
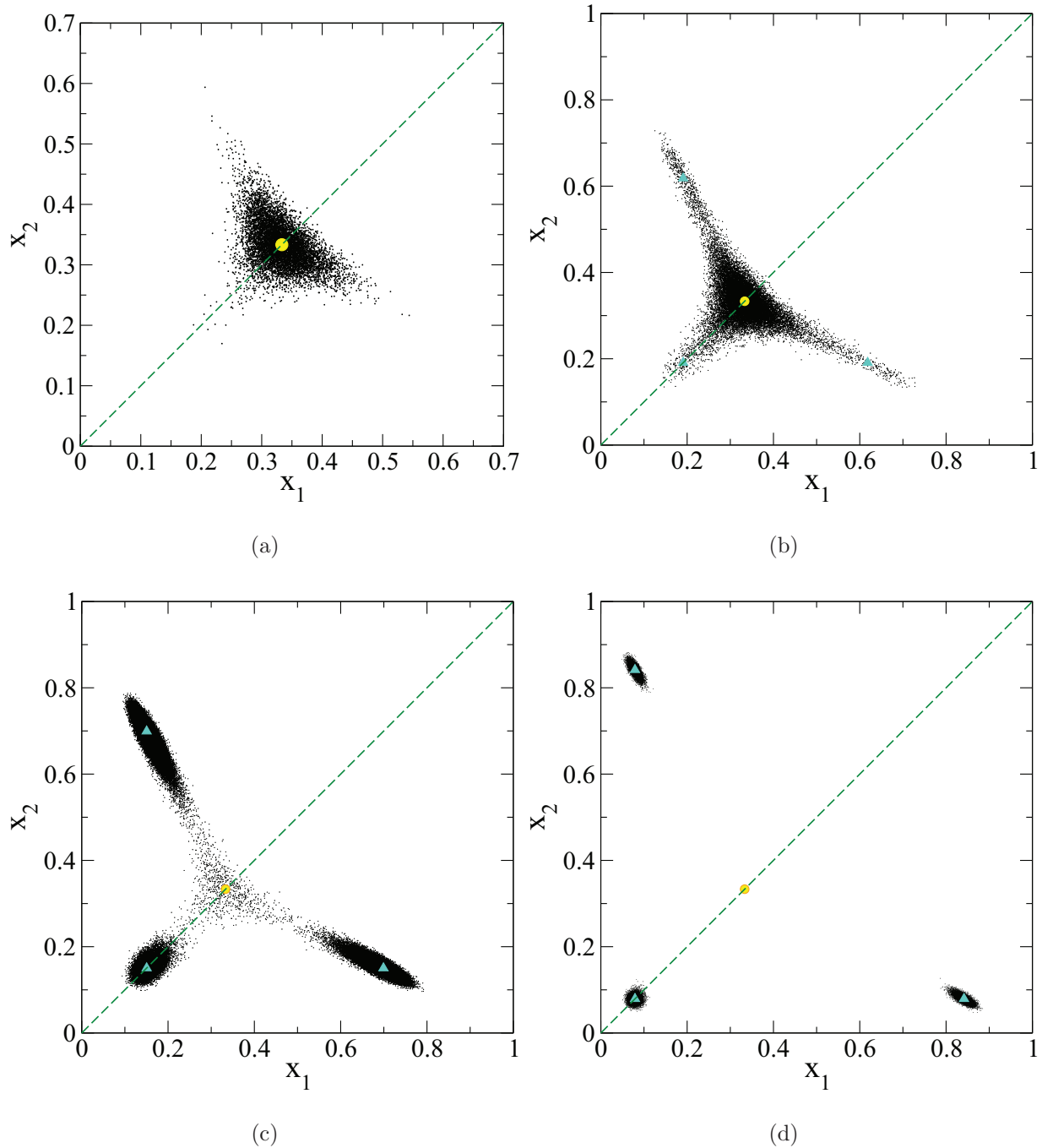
FIG. 5. Monte Carlo simulation results for the population distribution map of the three-urn model with $N = 3000$ at equilibrium. (a) $g = -2.7$ in the uniform state. (b) $g = -2.75$ and (c) $g = -2.8$ in the coexisting regime. (d) $g = -3.1$ in the nonuniform state. The uniform phase of $x_i = \frac{1}{3}$ is denoted by the yellow filled circle and the nonuniform phase is denoted by filled triangles.

function of g for the four-urn system at equilibrium. For low attractive strengths, the urns are equally populated with $\langle x_i \rangle \simeq \frac{1}{4}$. As the interparticle attraction increases across the predicted first-order transition point [$g_t = -3 \ln 3 = -3.29584$ from Eq. (29)], the populations become inhomogeneous when one urn is more populated and the other three are less but equally populated. The mean nonuniformity of the system $\langle \psi \rangle$ also shows a sharp rise as shown in Fig. 4(d).

For $M = 3$, there are only two independent variables x_1 and x_2 and the population distribution can be visualized in the two-dimensional density maps shown in Fig. 5. For $g > g_c$ the population map has a single peak at the uniform state [Fig. 5(a)], and the nonuniform state emerges and coexist as $g \lesssim g_c$ [Fig. 5(b)]. As the interparticle attraction becomes stronger ($g_t < g < g_c$), the nonuniform population become more significant [Fig. 5(c)]. Finally, at $g < g_t$, the

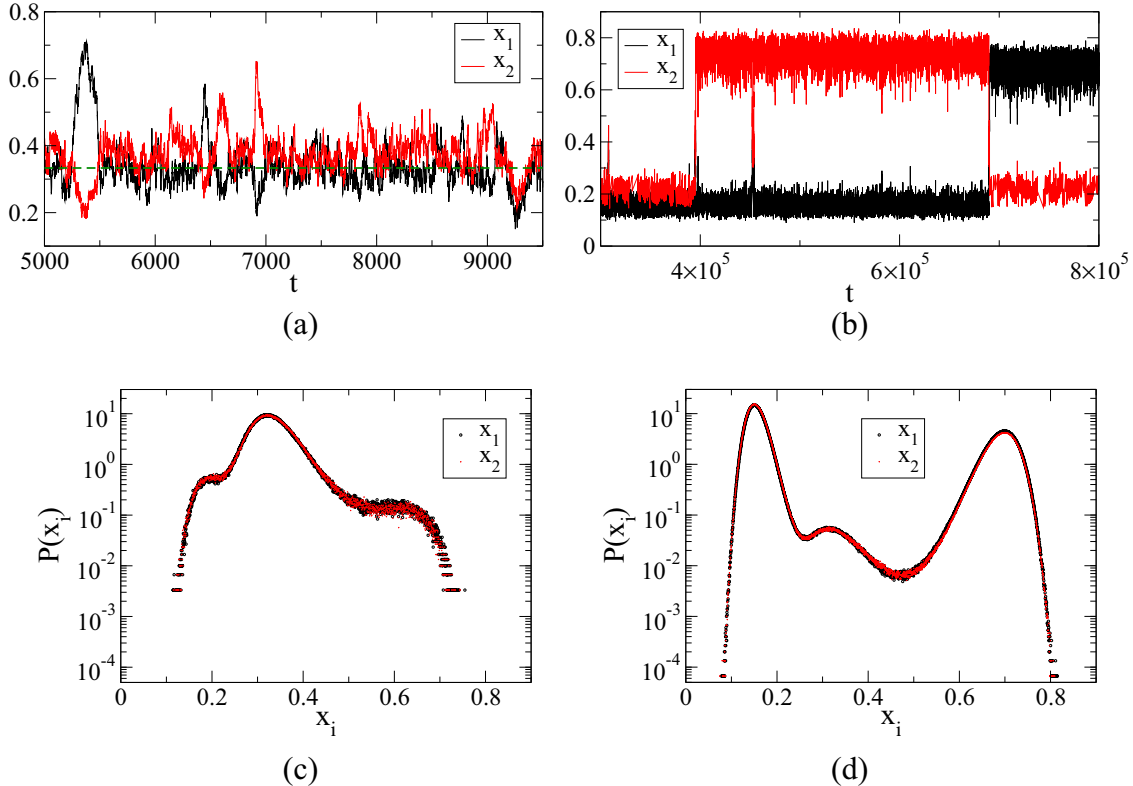FIG. 6. Monte Carlo simulation results for the time course of the populations in the three-urn model at equilibrium. $N = 3000$. The horizontal dashed line is the uniform state of $x_i = \frac{1}{3}$. Black (darker) curve shows x_1 and (grey) curve shows x_2. (a) $g = -2.75$ (b) $g = -2.8$ in the coexisting regime. Time in Monte Carlo Steps per particle (MCS/N). (c) $P(x_i)$ for the case in (a). 10^6 MCS/N are used. (d) $P(x_i)$ for the case in (b). 10^8 MCS/N are used to obtain good statistics.

uniform state vanishes and only the nonuniform phase remains [Fig. 5(d)].

The time courses of the population fractions of the three-urn system above and below the first-order transitions are shown in Figs. 6(a) and 6(b), respectively. For $g \gtrsim g_t$, the system spends most of the time around the uniform state with occasion hopping to the nonuniform metastable phases [Fig. 6(a)]. On the other hand, for $-3 < g < g_t$, the system is predominantly in the nonuniform phase but can hop between the degenerate permutation nonuniform phases in long timescales [Fig. 6(b)]. The coexistence of the uniform and nonuniform phases is explicitly spelled out in the distribution functions of each urn. As shown in Fig. 6(c), the system is dominated by the uniform phase with a prominent peak at $x_i = \frac{1}{3}$ but the two local peaks from the nonuniform phases are clearly seen. For $g < g_t$, the two peaks of the nonuniform phases grow at the expense of the uniform peak, as shown in Fig. 6(d).

VI. SUMMARY AND OUTLOOK

In this paper, the equilibrium properties of the Ehrenfest M-urn model with interparticle attractions within the same urn is investigated. It is shown that phases of different levels of population nonuniformity can exist, but only the uniform and the most nonuniform phases are locally stable. In addition, these two phases can coexist in a range of attraction strengths whose values can be calculated analytically. These

two phases are also connected by a first-order transition whose transition interaction strength [Eq. (29)] and energy barrier [Eq. (30)] can be derived explicitly for arbitrary values of M. For weak $|g|$, the system is in the symmetric (uniform) phase with the same mean population $x_i = 1/M$, and for strong $|g|$, the system is the asymmetric phase, and the only stable asymmetric phase is the ($k = 1$) most nonuniform state. This first-order phase transition is associated with the breaking of Z_M symmetry as $|g|$ is increased.

The theoretical findings are further verified by Monte Carlo simulations and the agreement is excellent. It is remarkable that as the interparticle attraction increases, the population changes from the entirely uniform state (in which entropy effects dominates) to the case with the emergence of the locally stable most nonuniform $k = 1$ state (in which energy dominates), rather than emerging with a less (or least) nonuniform state. And when the attraction is increased further, less nonuniform states ($k > 1$) can emerge, but they are all proved to be unstable. As a result, the most nonuniform state persists and remains stable for $g < g_c(n = 1)$ due to the domination of the all-to-all interparticle attractions within the urn over the entropy effects. These analytical results and physical picture can enhance our fundamental understanding of equilibrium phase transitions with multiphase coexistence.

The present model can be extended to the case in which the particles can possess internal energy levels. For instance, suppose that the energy spacing of the energy levels at each urn are the same, with the lowest one being zero. Now

consider the coupling constant to be negative so the particles interaction is attractive. When the temperature is lowered to zero, g approaches to $-\infty$. In this case, inside an urn, the occupation will be dominated by its lowest energy-level state. Because of mutual attraction between particles in the same urn, the total number of particles will be located at the lowest energy level of a specific urn. Hence, if one generalizes the classical particles to Bosons, also assuming the weak coupling regime and the transition between different urns is classical (no coherence between different urns), then it could possibly lead to Bose condensation in a specific urn.

Here we focused on the equilibrium behavior in which detailed balance is obeyed. But by allowing the jump rates between a pair of urns to be unbalanced, for instance in a one-dimensional ring, the clockwise and anticlockwise jump rates are p and q, respectively, with $p > q$, then a nonequilibrium state with a net clockwise flux results. With the particle interaction explicitly imposed in the model, the interplay of energy and entropy can lead to interesting equilibrium and nonequilibrium phase transitions. For example, although the less nonuniform states are found to be unstable, it may be plausible to stabilize them if the interurn interactions are introduced in a proper way. On the other hand, our model can also be extended to other nonequilibrium cases, such as by allowing the particles in the urns be active particles modeled by noise with nontrivial correlations or the particles are subjected to noises with nontrivial spectrum, then it may lead to additional contributions that could affect the breaking of the ergodicity [26,27] in the broken-symmetry nonuniform states. These systems are intrinsically nonequilibrium in nature, which is beyond the scope of the present study, but can be investigated in future.

Finally, we emphasize that the M urn with the interaction model can serve as a new paradigm model to study various nontrivial equilibrium and nonequilibrium statistical mechanics in a more analytically tractable way, including nonequilibrium steady states or even far from equilibrium situations such as oscillations and even complex spatial-temporal patterns. These are under our current investigations and the results will be presented in future publications.

ACKNOWLEDGMENTS

APPENDIX: STABILITY CALCULATIONS FOR THE NONUNIFORM PHASES

In this Appendix, we give more details on the definitions of the nonuniform phases and derive their stability conditions. The possible phases are given by the roots of x in the saddle point Eqs. (8). As discussed in Sec. II A, the function xe^{gx} can have at most two distinct values for $0 \leqslant x \leqslant 1$, thus at equilibrium the population fractions can only take at most two possible values for a given value of g. Hence we define the kth phase as the particle distributions such that there are k urns with the same occupation fraction, say y, and the rest $(M - k)$ of the urns have the same population fraction, say x. Thus it

follows that the kth and phases are the same and it suffices to consider $k = 0, 1, \cdots, \lfloor \frac{M}{2} \rfloor$ possible phases. In general, $x \neq y$ and $k \neq 0$ for the nonuniform phases, otherwise a uniform phase results. It would be more intuitive to rewrite Eqs. (8) as

$$xe^{gx} = ye^{gy}, \tag{A1}$$

$$x = \frac{1 - (M - k)y}{k}, \tag{A2}$$

where the relation between x and y in Eq. (A2) simply follows from the requirement that the sum of all population fractions must be unity. Since the system possesses permutation symmetry of the M identical urns, one has the freedom to choose the independent coordinates $x_1, x_2, \cdots, x_{M-1}$, i.e., freedom to label the urns using distinct labels. For actual calculations, we need to choose a convenient labeling. For instance, one can choose the kth phase as given by the $M - 1$ component vector,

$$\vec{x}^{(k)} = (y, \cdots, y, x \cdots, x)^\mathsf{T} \qquad 1 \leqslant k \leqslant \left\lfloor \frac{M}{2} \right\rfloor, \tag{A3}$$

whose first $M - k$ components have the same value y (but $y \neq \frac{1}{M}$) and the rest of the $k - 1$ components have the same value of $x = \frac{1-(M-k)y}{k}$. The value of y can be solved by substituting Eq. (A2) into Eq. (A1) to give

$$ky = [1 - (M - k)y]e^{\frac{g}{k}(1-My)}. \tag{A4}$$

The nonuniformity of the kth phase can be computed from Eq. (32) to be

$$\psi^{(k)} = \sqrt{\frac{2}{M(M-1)}\left(\frac{M}{k} - 1\right)}|1 - My|. \tag{A5}$$

In the strong attraction limit, $g \to -\infty$, Eq. (A4) gives $y \simeq \frac{e^{-|g|/k}}{k} \to 0$ and $\psi^{(k)}(g \to -\infty) \simeq \sqrt{\frac{2}{M(M-1)}\left(\frac{M}{k} - 1\right)}(1 - \frac{M}{k}e^{-|g|/k}) \to \sqrt{\frac{2}{M(M-1)}\left(\frac{M}{k} - 1\right)}$, which is a decreasing function in k. Thus the first nonuniform phase ($k = 1$) is the most nonuniform state.

Apart from the uniform saddle point $\frac{1}{M}$, there are in general two nonuniform roots of y from Eq. (A4). More insight can be gained by examining the x-y plane unit square (see Fig. 7) in which the intersection of the curve Eq. (A1) and the line Eq. (A2) gives the roots for the saddle points. Consider the case of $x \neq y$ and $k \neq 0$ (nonuniform phases) and $g < -1$, it can be shown [28] that the curve Eq. (A1) always lies outside the square boxes $[0, -\frac{1}{g}] \times [0, -\frac{1}{g}]$ and $[-\frac{1}{g}, 1] \times [-\frac{1}{g}, 1]$, and hence the saddle point must satisfy the condition that one of the x or y is $> -\frac{1}{g}$ (but not both), and the other one is $< -\frac{1}{g}$.

1. Instability for the $k \geqslant 2$ phases

Here we compute the eigenvalues of Hessian matrix at the kth nonuniform saddle-point which is given by the root of the saddle-point equation (9). The stability condition of the kth phase is determined by the $(M - 1) \times (M - 1)$ Hessian matrix from Eqs. (18) and can be computed by choosing saddle-point $\vec{x}^{(k)}$ as in Eq. (A3) to give

$$\left.\frac{\partial^2 f}{\partial x_\alpha \partial x_\beta}\right|_{\vec{x}^{(k)}} = -\left[\frac{1}{x} + g\right] - \left[\frac{1}{y} + g\right]\delta_{\alpha\beta}, \tag{A6}$$
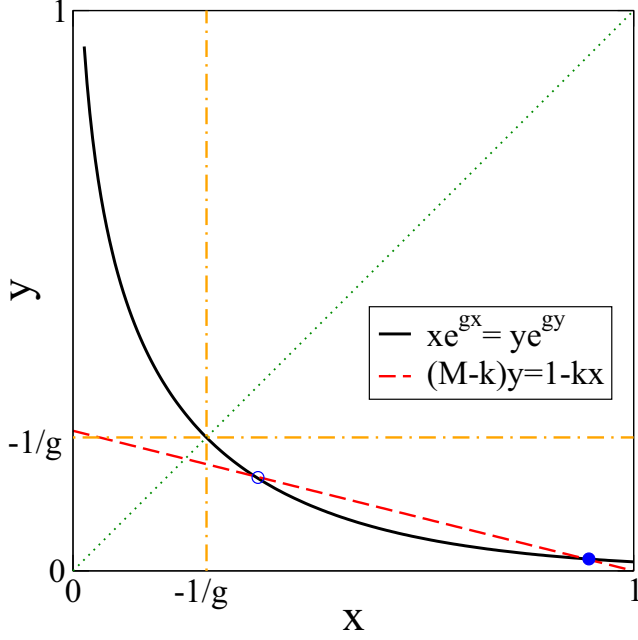
FIG. 7. Plots of the curve Eq. (A1) (for $x \neq y$) and the line Eq. (A2). The two intersections at $x = x_+$ and $x = x_-$ are indicated by filled and open circles, respectively. The $x = -\frac{1}{g}$ and $y = -\frac{1}{g}$ are indicated by dot-dashed lines. The $x = y$ line is indicated by the dotted line.

whose eigenvalues can be solved [29] to give (for $2 \leqslant k \leqslant \lfloor \frac{M}{2} \rfloor$)

$$\lambda_B \equiv -\left(\frac{1}{y} + g\right) \quad \text{[with } (M - k - 1) \text{ degeneracy]}, \quad (A7)$$

$$\lambda_A \equiv -\left(\frac{1}{x} + g\right) \quad \text{[with } (k - 2) \text{ degeneracy]}, \quad (A8)$$

$$\frac{1}{2}\{M\lambda_A + \lambda_B \pm \sqrt{(M\lambda_A + \lambda_B)^2 - 4\lambda_A[(M - k)\lambda_A + k\lambda_B]}\}. \quad (A9)$$

These eigenvalues depend on the roots x and y which in turns depend on g. Now it is easy to see for $k \geqslant 3$, since one of the x or y is $> -\frac{1}{g}$ and hence either λ_A or λ_B is positive, thus rendering these phases to be always unstable. λ_A is absent for $k = 2$, but we can choose another convenient coordinate such as

$$\vec{x}^{(k)} = (x, x, y, \cdots, y)^\mathsf{T} \quad (A10)$$

and one can compute directly to see that both λ_A and λ_B are eigenvalues and hence the $k = 2$ phases are also unstable.

2. Stability and instability for the $k = 1$ phases

For $k = 1$, it is convenient to choose the coordinate such that

$$\vec{x}^{(1)} = (y, \cdots, y)^\mathsf{T} \quad (A11)$$

and $x = 1 - (M - 1)y$. One can compute directly to find the eigenvalues to be λ_B [with $(M - 2)$ degeneracy] and $\Lambda \equiv (M - 1)\lambda_A + \lambda_B = -Mg - \frac{M-1}{x(1-x)}$, where λ_A and λ_B are given as in Eqs. (A8) and (A7). For $g < g_c(n = 1) \equiv g_c$, two $k = 1$ phases emerge with the corresponding roots x_+ and x_- via saddle-node bifurcation, which occurs at $x = x_c$. As g is further decreased, x_+ keeps increasing while x_- keeps decreasing. As discussed in previous subsection, $\lambda_B > 0$ if the root $x < -\frac{1}{g}$ and $\lambda_B < 0$ if $x > -\frac{1}{g}$. Since the stability also depends on the sign of Λ, we first find out the conditions that $\Lambda = 0$. Vanishing Λ occurs for x satisfying $x = \frac{1-x}{M-1}e^{-\frac{1-Mx}{Mx(1-x)}}$. Careful examination of the roots of this equation reveals that there are two roots at $x = x_c$ (the saddle-node bifurcation point at $g = g_c$) and at $x = x_- = \frac{1}{M}$ (which occurs at $g = -M$). The eigenvalues λ_B and Λ evaluated at x_+ and x_- determine the stability of these two phases, which are considered for the following two regimes in g.

a. $-M \leqslant g < g_c$

We first consider the case of weaker interparticle attraction $-M \leqslant g < g_c$. The condition for saddle-node bifurcation gives the relation between g_c and x_c: $M - 1 = -g_c M x_c(1 - x_c)$, which in turn shows the eigenvalue $\Lambda|_{x_c} = 0$ at the saddle-node bifurcation point. For $g < g_c$, two roots $x_+ > x_c$ and $x_- < x_c$ emerge, and we will show the corresponding eigenvalues $\Lambda|_{x_+} < 0$ $\Lambda|_{x_-} > 0$ in this regime of g. As g becomes more and more negative, x_- decreases and at $g = -M$, $x_- = \frac{1}{M}$, and the corresponding eigenvalue $\Lambda = 0$. Since $\Lambda|_{x_-} = 0$ occurs only at $g = g_c$ and $g = -M$, thus $\Lambda|_{x_-}$ does not change signs in the $-M \leqslant g < g_c$ region. Similarly, $\Lambda|_{x_+}$ will not change sign in the $g < g_c$ region.

We now use perturbation to show that for $g \lesssim g_c$, $\Lambda|_{x_+} < 0$ and $\Lambda|_{x_-} > 0$. With $g = g_c - \epsilon$ and writing $x \simeq x_c + \delta$, expanding the saddle-point equation to leading order in ϵ gives $\delta^2 = \frac{2x_c^2(1-x_c)^2(Mx_c-1)}{(M-1)(2x_c-1)}\epsilon$. Thus we have

$$\Lambda|_{x_\pm} = \mp \frac{2x_c - 1}{x_c^2(1 - x_c)^2}(x_\pm - x_c), \quad (A12)$$

and hence $\Lambda|_{x_+} < 0$ and $\Lambda|_{x_-} > 0$ once the saddle-node bifurcation occurs. Since $\Lambda|_{x_-}$ does not change signs in the regime of g, x_- is unstable. For x_+, $\Lambda|_{x_+}$ also does not change signs and remains < 0, also the other eigenvalue $\lambda_B < 0$ (since $x_+ > -\frac{1}{g}$ and $y_+ < \frac{1}{g}$), thus it is stable.

b. $g < -M$

In this case, $x_- < -\frac{1}{g}$ and its eigenvalue $\lambda_B > 0$ and this phase is unstable. On the other hand, x_+ remains $> -\frac{1}{g}$ and both of its eigenvalues $\lambda_B < 0$ and $\Lambda|_{x_+} < 0$, ensuring that this is a stable phase.

[1] L. Boltzmann, Trans. Acad. Sci. **66**, 275 (1872).

[2] K. Huang, *Statistical Mechanics*, 2nd ed. (Wiley, New York, 1987).

[3] P. Ehrenfest and T. Ehrenfest, Phys. Z. **8**, 311 (1907).

[4] M. Kac, Am. Math. Mon. **54**, 369 (1947).

[5] A. J. F. Siegert, Phys. Rev. **76**, 1708 (1949).

[6] M. J. Klein, Phys. Rev. **103**, 17 (1956).

[7] D. L. Iglehart, Ann. Math. Stat. **39**, 864 (1968).

[8] Y. M. Kao and P. G. Luan, Phys. Rev. E **67**, 031101 (2003).

[9] Y. M. Kao, Phys. Rev. E **69**, 027103 (2004).

[10] J. Nagler, Phys. Rev. E **72**, 056129 (2005).

[11] J. Nagler, C. Hauert, and H. G. Schuster, Phys. Rev. E **60**, 2706 (1999).

[12] E. M. F. Curado and F. D. Nobre, Phys. Rev. E **67**, 021107 (2003).

[13] F. D. Nobre, E. M. F. Curado, and G. Rowlands, Phys. A **334**, 109 (2004).

[14] G. A. Casas, F. D. Nobre, and E. M. F. Curado, Phys. Rev. E **91**, 042139 (2015).

[15] J. P. Bouchaud and A. Georges, Phys. Rep. **195**, 127 (1990).

[16] J. P. Boon and J. F. Lutsko, Europhys. Lett. **80**, 60006 (2007).

[17] J. F. Lutsko and J. P. Boon, Phys. Rev. E **88**, 022108 (2013).

[18] V. Schwammle, F. D. Nobre, and E. M. F. Curado, Phys. Rev. E **76**, 041123 (2007).

[19] M. Shiino, J. Math. Phys. **42**, 2540 (2001).

[20] T. D. Frank and A. Daffertshofer, Phys. A **295**, 455 (2001).

[21] P. H. Chavanis, Phys. Rev. E **68**, 036108 (2003).

[22] B. Meerson and P. Zilber, J. Stat. Mech. (2018) 053202.

[23] C. H. Tseng, Y. M. Kao, and C. H. Cheng, Phys. Rev. E **96**, 032125 (2017).

[24] P. Y. Lai and Y. Y. Goldschmidt, J. Stat. Phys. **48**, 513 (1987).

[25] Y. Y. Goldschmidt and P.-Y. Lai, J. Phys. A **21**, L1043 (1988).

[26] M. H Lee, Phys. Rev. Lett. **98**, 190601 (2007).

[27] L.C. Lapas, R. Morgado, M. H. Vainstein, J. M. Rubí, and F. A. Oliveira, Phys. Rev. Lett. **101**, 230602 (2008).

[28] Without loss of generality, take $\frac{y}{x} < 1$; Eq. (A1) gives $z = e^{gx(1-z)}$, where $z \equiv \frac{y}{x} < 1$. It follows that $gx < -1$ for the above equation to hold, i.e., $x < -\frac{1}{g}$. Similarly, one can also write Eq. (A1) as $z = e^{gy(1-z)}$, where $z \equiv \frac{x}{y} > 1$, now $gy > -1$ for the above equation to hold, i.e., $y > -\frac{1}{g}$ also. One can repeat the argument by taking $\frac{y}{x} > 1$, which leads to the condition of $x > -\frac{1}{g}$ and $y < -\frac{1}{g}$. Hence the curve Eq. (A1) for $x \neq y$ lies in the region where one of the x or y (exclusively) is $> -\frac{1}{g}$ and the other one is $< -\frac{1}{g}$. See Fig. 7.

[29] The following formula for the determinant is useful to compute the eigenvalues:

$$
\mathcal{M} = \left.\left(\begin{array}{ccc|ccc} C & & A & A & \cdots & A \\ & \ddots & & & \ddots & \\ A & & C & A & \cdots & A \\ \hline A & \cdots & A & X & & A \\ & \ddots & & & \ddots & \\ A & \cdots & A & A & & X \end{array}\right)\right\}\begin{array}{l}\\ n-s \\ \\ \\ s\\ \end{array}
$$

$$
\det \mathcal{M} = (-1)^s (C-A)^{n-s-1}(A-X)^{s-1}\{A[(n-1)A-(s-1)C]
$$
$$
-X[(n-s-1)A+C]\}.
$$